JOURNAL OF MATERIALS SCIENCE **39** (2004) 5905–5913

High speed propulsion: Performance advantage of advanced materials

T. A. JACKSON, D. R. EKLUND, A. J. FINK
Air Force Research Laboratory, Wright-Patterson AFB, OH, USA
E-mail: thomas.jackson@wpafb.af.mil

High-speed air breathing propulsion systems have many attractive military and civil applications. The high propulsive efficiency of these systems allows the exploitation of speed, distance, and bigger payloads, or any combination of the three. The severe operating conditions of these systems require particular attention to overall thermal management of the engine/air-frame. Fuel-cooling the engine structure is a viable way of maintaining thermal balance over a range of flight conditions. Air Force applications have focused on using endothermic hydrocarbon fuels to address this issue because of their compatibility with the military operations. Recent ground tests of scramjet engines have demonstrated adequate performance utilizing state-of-the-art technology in materials. This progress has paved the way for an expendable flight test vehicle in the near future. In order to take full advantage of the capabilities of this propulsion system, advances in fuel-cooled structures, high temperature un-cooled materials, and increased heat capacity of hydrocarbon fuels will be needed to enable expendable systems to reach higher Mach numbers. An additional benefit would be realized in future reusable systems.

1. Introduction

Speed has its advantages. The speed to escape a threat, to defeat a time-critical target, to gather information rapidly, and to launch a package to space all follow from high-speed propulsion technology [1]. The rocket is a high-speed propulsion device, long used for short range weapons and for access to space. In carrying all its required propellants, however, rocket-powered devices have low specific impulse (thrust per rate of mass propellant burned). Turbine engine technology, high in specific impulse, is limited in the range of Mach numbers over which it can operate. Ramjets and scramjets (supersonic combustion ramjet) offer a means of achieving high specific impulse over a broadened range of flight Mach numbers, Fig. 1 [2].

Hydrogen offers the widest range of utility given the parameters of Fig. 1. However, vehicle volume constraints generally dictate this fuel be stored and used as a cryogen. For flexibility in storage, basing, and pace of operations, and for high density in packaging on the air vehicle, conventional aviation hydrocarbon fuels are being developed for high speed propulsion engines up to flight Mach number of 8 to 10. The upper speed limit is determined by the ability of the fuel to manage the thermal load of the engine/air-frame structure.

Fuel is routinely used in aviation to maintain thermal balance. Subsonic and supersonic, turbine engine powered systems use the latent heat capacity of the fuel to cool avionics, crew environment, and engine oil. Standard aviation fuel is heated up to 435 K prior to injection into the engine combustor. The SR-71 Blackbird flew at speeds exceeding Mach 3 and used a more specialized fuel, JP-7, to maintain acceptable structural temperatures. It relied only on the heat capacity of the liquid fuel for the heat sink. Above the speeds of the Blackbird, aero-heating is more severe and reusable components must be more aggressively cooled. Endothermic fuels were introduced as an advanced heat sink approach in the 1960's [3, 4]. These fuels are designed to decompose within the fuel system under extreme heating. The process essentially quadruples the available heat capacity of distillate hydrocarbon fuels. Expendable systems currently under development would exploit this broadened heat capacity to push fuel-cooled structures to Mach 7. Pushing expendable systems further, and supporting reusable structures from Mach 4 and up, will require advanced fuel-cooled structures, a higher percentage of un-cooled, heat-tolerant components, and continued advancement of high heat-sink fuels.

This paper addresses high-speed, air-breathing flight up to Mach 8. It also focuses on hydrocarbon fuelled engines. Higher speeds exacerbate the challenges; hydrogen fuel mitigates these somewhat, but introduces other challenges noted earlier. We'll leave such considerations for other authors.

2. Flight environment

2.1. Engine conditions

The engine environment changes as the vehicle accelerates and climbs. A representative altitude-Mach number corridor is depicted in Fig. 2. Overlaid on the figure

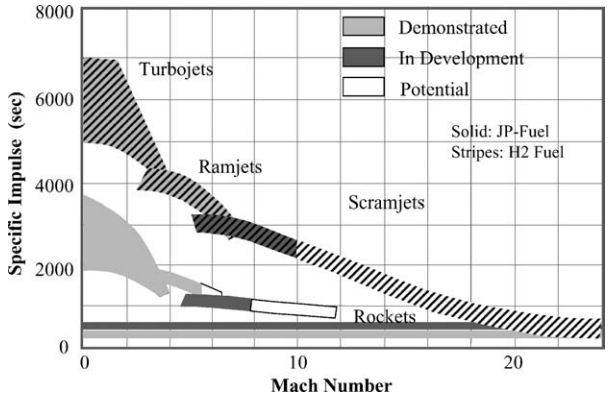

Figure 1 Comparison of propulsion cycles, Mach 0 to 25.

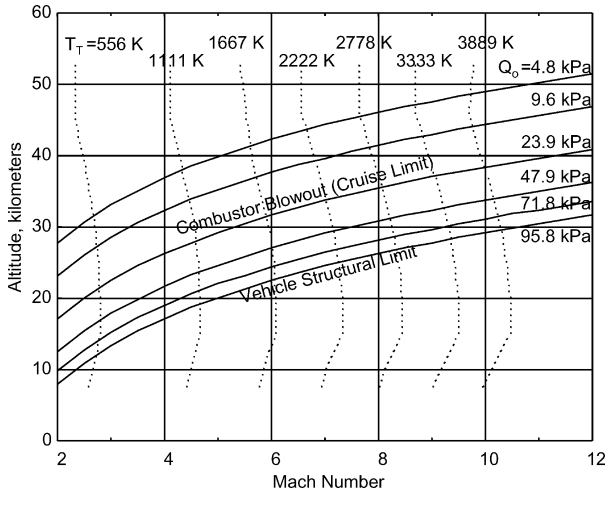

Figure 2 Flight corridor of an air-breathing, high-speed vehicle through Mach 12.

are lines of constant total temperature (T_T). The lower altitude limit is set by vehicle structural considerations, with dynamic pressure (Q_0) generally held to a maximum of 95 kPa (reusable) to 150 kPa (expendable); the upper limit is set by the combustion stability, which degrades with decreasing pressure.

The ramjet and scramjet engines function by controlling flow areas. The inlet and portions of the vehicle forebody are designed to capture, compress, and decelerate the free-stream air. The combustor adds energy to the flow though fuel-air burning. The exhaust nozzle accelerates and expands the flow toward free-stream pressure. The ramjet is configured to operate fully subsonic within the combustor. It forces this condition by incorporating a physical restriction or throat between the combustor and exhaust nozzle. The scramjet has no such physical restriction; heat release provides sufficient flow restriction to choke the flow, generating a shock train upstream of the heat release. This results in subsonic combustion, mimicking a ramjet environment. At higher flight Mach numbers the heat release is insufficient to choke the flow and it remains supersonic everywhere in the engine except in the vicinity of the flame holder. Above approximately Mach 6 the scramjet is the desired engine cycle. Decelerating the Mach 6 flow to subsonic speeds would raise the local static temperature to 1600 K and induce large losses in total pressure, and increase structural loads.

Internal scramjet conditions, including static and total pressures and temperatures and the local velocity and Mach number, are tabulated at key engine stations below the schematic of Fig. 3. These conditions are representative of the steady state, combusting conditions at two flight Mach numbers (M_0). The flow-path configuration is an Air Force research design, incorporating a cavity flame-holder and angled, flush-wall fuel injectors. The combustor is ethylene fueled and has been experimentally evaluated through Mach 5.5 in direct-connect testing. For the two conditions tabulated the equivalence ratios $((f/a)_{\text{actual}}/(f/a)_{\text{stoichiometric}})$ are 1.0 and 0.94 for flight Mach numbers 4.0 and 6.5, respectively. Inlet and exhaust nozzle characteristics are based on standard design practice and are analytical only, not based on experiment.

Heat flux to the engine structure is substantial. It has been computed for the research flow-path at the Mach 6.5 condition. Symmetry was assumed and one-half of the combustor is displayed in Fig. 4. Heat release from combustion causes the flow to separate approximately 2.5 duct heights upstream of fuel injection. A sizable region of the duct near the top and side walls and downstream of the fuel injectors is characterized by recirculating or low velocity flow. Nevertheless, the average Mach number exceeds 1.5 throughout the combustor. Temperature contours reveal that the recirculation zone along the side wall acts as a flameholder in addition to the cavity on the vehicle body side. The calculation employed a coupled 1-D fluid/solid interface heat flux model. The surface of the combustor was assumed to be steel with a thickness of 0.254 cm and a conductivity of 28.3 W/m K. In the simulation the combustor was assumed to be water-cooled with a backside temperature equal to 300 K. The surface heat flux distribution is shown in the figure along the top and side walls. Note the elevated heat flux values along the side wall due to contact with hot combustion products. Along the top wall the heat flux is also observed to increase downstream of the cavity due largely to the higher flow velocities in this region. The heat flux varies significantly through the combustor due to the local flow conditions, which complicates cooling strategies.

2.2. Endothermic fuel environment

Fuel is routinely used to cool aviation engines. In conventional systems, operating below Mach 3, fuel cooling is done through the engine's fuel-oil heat exchanger; fuel is not circulated through the engine structure itself. The maximum operating temperature of the fuel is set carefully so as not to induce the formation of solids within the fuel system that could adversely affect flow. Heating the fuel from tank temperature to this limit yields approximately two hundred cal/gm-fuel heat capacity. Further heating in the presence of a suitable catalyst will break the original fuel down to lower molecular weight hydrocarbons and molecular hydrogen. Original work on these *endothermic* fuels focused on pure hydrocarbons. Methylcyclohexane (MCH) for instance converts to toluene and hydrogen

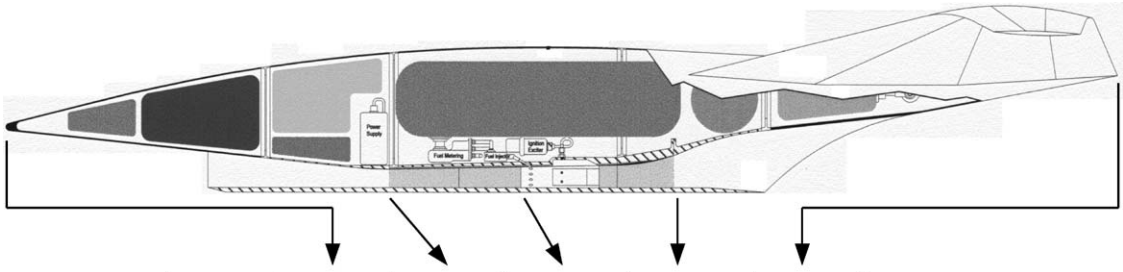

Enigne Station	Free Stream	Inlet Throat	Combustor Entrance	Combustor Exit	Nozzle Exit
	M_o = 4.0, Q_o = 47.9 kPa (21.7 km)				
P_s (kPa)	4.23	59.8	204.9	124.8	4.23
P_T (kPa)	676	650	433	270	251
T_s (K)	218	474	718	1691	675
T_T (K)	891	883	860	1949	1926
M	4.00	2.18	1.02	1.12	3.74
V (m/s)	1189	944	531	845	1867
	M_o = 6.5, Q_o = 47.9 kPa (28.1 km)				
P_s (kPa)	1.59	65.9	59.3	105.0	1.59
P_T (kPa)	5386	2366	2044	588	446
T_s (K)	225	781	779	1902	717
T_T (K)	1902	1747	1709	2521	2402
M	6.50	2.86	2.81	1.68	4.12
V (m/s)	1959	1549	1516	1341	2156

Figure 3 The scramjet flow environment for flight Mach numbers 4.0 and 6.5.

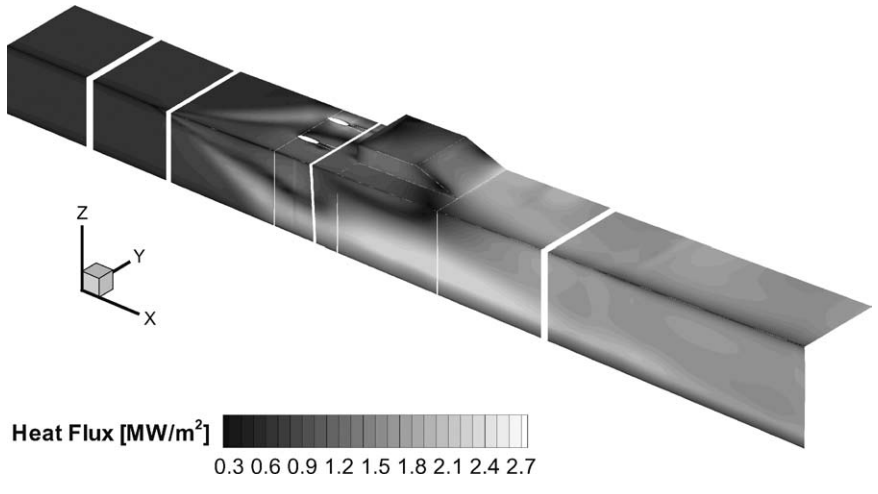

Figure 4 Heat flux to a scramjet at simulated Mach 6.5 flight conditions.

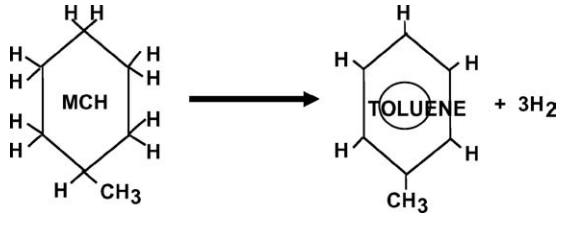

Figure 5 Full endothermic conversion of Methylcyclohexane.

as shown in Fig. 5, absorbing over 500 cal/gm-fuel in the process. The lighter hydrocarbons of the break-down products can be heated further, utilizing their latent heat capacity. The entire heating process for typical distillate hydrocarbon fuels absorbs 800 to 1100 cal/gm-fuel in contrast to the 160 cal/gm-fuel of the more conventional liquid-heating approach.

A fuel-cooled scramjet takes advantage of the full cooling capacity of the fuel. JP7 is the current fuel of choice. It is a highly refined middle distillate fuel with excellent thermal properties. To maintain thermal balance of the scramjet structure, JP7 is substantially heated, forcing it to undergo thermodynamic and composition changes. At Mach 4 the fuel is supercritical JP7; at Mach 6 a partially cracked mixture of JP7 and lighter hydrocarbons; and at Mach 8 a fully cracked mixture of light hydrocarbons with the fuel's total thermal capacity spent. At some point during the cracking process the thermodynamics have shifted such that the fuel is superheated vapor, below critical pressure and can be treated as an ideal gas. In current, prototype systems the fuel is assumed to always behave as an ideal gas in designing and positioning fuel injectors.

Fig. 6 illustrates the expected shift in the two-phase dome as the fuel is cracked. Depicted are the two-phase domes for the unreacted, high molecular weight JP-7 (smaller dome), and the partially cracked mixture of low molecular weight hydrocarbons and unreacted

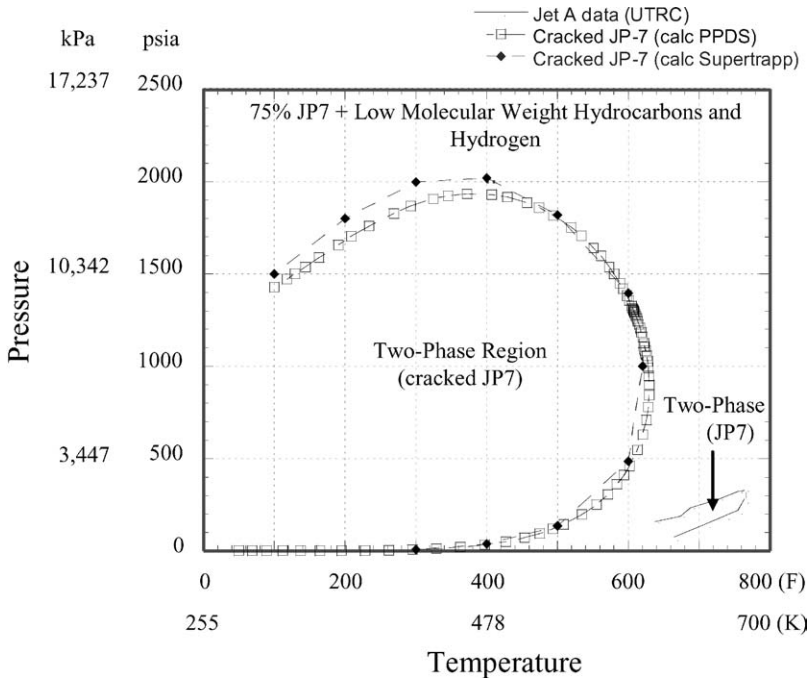

Figure 6 Pressure-Temperature phase diagram for JP7, neat and cracked.

JP-7. The smaller dome characterizes the fuel at engine start and lower flight Mach numbers. Its shape is estimated from Jet-A (commercial aviation fuel) data. The larger dome is more representative of the fuel in the system under the high thermal stress of high Mach numbers. Its shape is computed. Fuel manifold pressure is held fairly constant. Fuel temperature varies. And, the critical point changes with the composition. The behavior of the injectant varies depending on the pressure/temperature conditions relative to the appropriate critical point and two-phase dome.

This process of active cooling has additional system benefits. The fuel entering the combustor is more energetic, with the gravimetric heat of combustion increased by 10%. And, the expected break-down products generally are more readily burned than the parent molecules. Decomposition products are not available for JP7, but they are for an enhanced thermal stability aviation turbine engine fuel, JP8+100 [5]. Table I lists the major species of the decomposition of this fuel. Both JP7 and JP8 are middle distillates and decomposition products are expected to be similar.

In a reusable, broad operating range application the hydrocarbon fuel will go through phase and composition changes in meeting the thermal balance needs of the engine and vehicle. Without pre-heating the fuel will be liquid at scramjet take-over, super-critical at some intermediate Mach number, and a super-heated, low molecular weight gas at the highest flight Mach number. The process is a continuum but the three distinct stages have been studied in terms of injector performance. These stages are illustrated in Fig. 7.

TABLE I Decomposition products of JP8+100 at 968 K (estimated from Fig. 6 of Ref. [5])

Molecule	H_2	CH_4	C_2H_4	C_2H_6	C_3H_6	C_3H_8	C_4H_8	C_4H_{10}
Mol%	7	22	16	21	15	10	7	2

Aerating the liquid hydrocarbon fuel is very effective in promoting rapid atomization and dispersion of the fuel. Ignition and sustained combustion at Mach 4 flight conditions have been demonstrated in direct connect testing; and the mechanics of the process studied extensively [6]. Fig. 7a is a photograph of the injector internal flow. Gas is injected into the liquid through discrete holes in a tube centered within the injector body. The flow transitions from discrete gas bubbles to a stable, central gaseous core surrounded by a liquid sheet. The high speed gaseous core is very effective at increasing liquid fuel penetration into the supersonic cross-flow and destabilizing the liquid sheet to accelerate atomization. Less than five weight percent of gas is sufficient to drive the injection/atomization process.

At higher structural heat loads the fuel is heated beyond its critical temperature. Transport from the collection manifolds in the fuel-cooled structure through the engine plumbing and metering equipment drops the fuel temperature. Expansion through the injector drops the pressure, further decreasing the fuel's static temperature. The supercritical fuel can condense during expansion into the combustor, Fig. 7b [7].

At still higher structural heating the fuel is well into the supercritical state and, upon cracking, moves into the superheated gas state. Injection is well predicted by ideal gas analysis. It takes the familiar shape depicted in Fig. 7c [7].

In current engine development programs such as the Air Force Hypersonic Technology (HyTech) effort we take the simplest injection approach and do what is necessary, typically fuel pre-heating, to keep the fuel in the ideal-gas-like state over the entire engine operating cycle. In combined cycle engines which will transition routinely from lower speed cycles, such as a gas turbine,

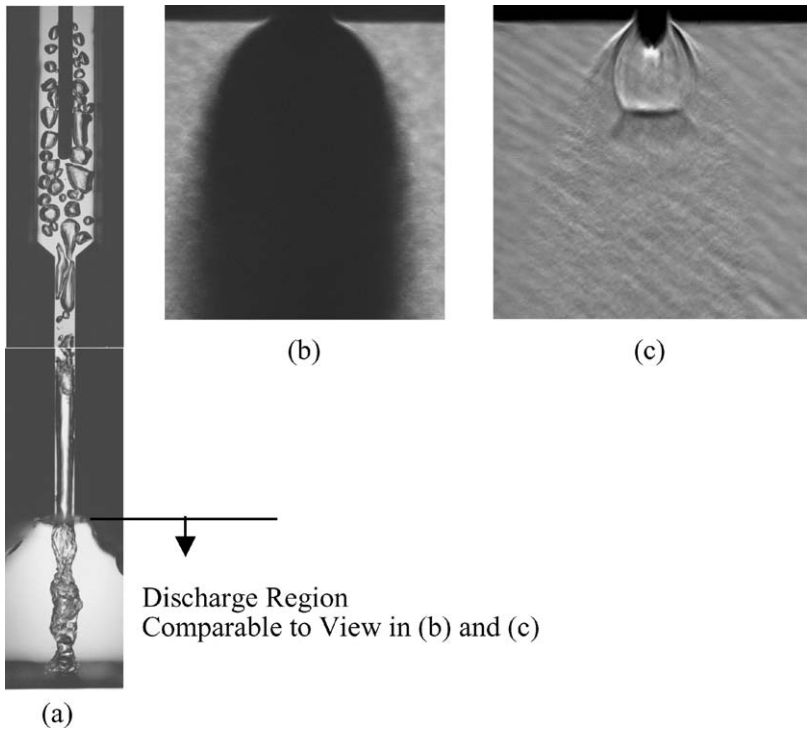

Figure 7 Three regimes of fuel injection: (a) aerated liquid, (b) supercritical to sub-critical phase transition, and (c) ideal gas.

to the high speed scramjet, and then back to low speed, managing the fuel in any possible state will become a priority.

2.3. HyTech engine

The Air Force has sponsored the HyTech engine development program since 1995. It will support the NASA/Air Force X-43C and Air Force Single Engine Demonstration (SED) flight test programs. The programs differ in their inlet geometry and flight test objectives. The X-43C is a large vehicle requiring three engine modules side-by-side. The inlet incorporates a movable cowl flap to aid in inlet starting and to optimize the contraction ratio as the vehicle accelerates. The SED is a single engine module and is entirely fixed geometry. Inlet starting is enabled by swept back sidewalls that offset the large inlet contraction ratio at the take-over Mach number. The X-43C and SED engines both rely on active, endothermic fuel cooling of engine structures along with a mix of un-cooled, high temperature components.

Fuel-cooled parts are fabricated from inconel plate. Channels are water-jet machined into the plate along the flow axis of the engine. Four such plates form the four sides of the engine. The engine cross-section is rectangular. An inconel sheet is placed over the exposed channels and laser welded to the plate. The sheet is welded to the plate along every land surface, forming closed box channels. These channels are coated with a catalyst to drive the endothermic decomposition of the fuel and retard or prevent coking. The four plate-sheet assemblies are either welded or bolted to each other to form the flow-path of the engine. The channels within the four walls run from fore to aft manifolds transporting the engine fuel flow through the inconel structure, keeping it in thermal balance. The fuel collected in the aft manifold is routed through metering valves and into various injector banks for combustion within the engine flowpath. An example of a section of fuel-cooled structure is depicted in Fig. 8. The large land surface in the middle will be the location of some engine case penetration such as a fuel injector, spark plug, or piece of flow-side instrumentation.

Un-cooled structures are constructed from silicon-carbide. It is used on leading edge surfaces such as the cowl and side-wall leading edges. It is formed to the desired shape and pinned to the adjacent cooled metal part. An example of a leading edge component is depicted in Fig. 9. Visible are the lines indicating the part was fabricated in three pieces and joined. For the expected duration of the mission (<20 min), and the expected number of thermal cycles (one) this part is expected to maintain shape and survive uncooled. Longer duration flights and certainly reusable applications will necessitate a different solution to the leading edge challenge.

3. With better materials and processes

The thermal environment for high-speed, air-breathing flight is very severe. The speed range described so far is through Mach 8. Our interest in air-breathing propulsion extends as high as Mach 15. Our focus has been on expendable systems, but our interests include reusable devices. Material and process development is at the heart of pushing the flight Mach number beyond 8, and developing reusable systems. Materials tolerant to higher operating temperatures and resistant to oxidation, and structures tolerant to thermal cycling and resistant to deformation would quickly find a place in the engine design. We can provide some detail as to how

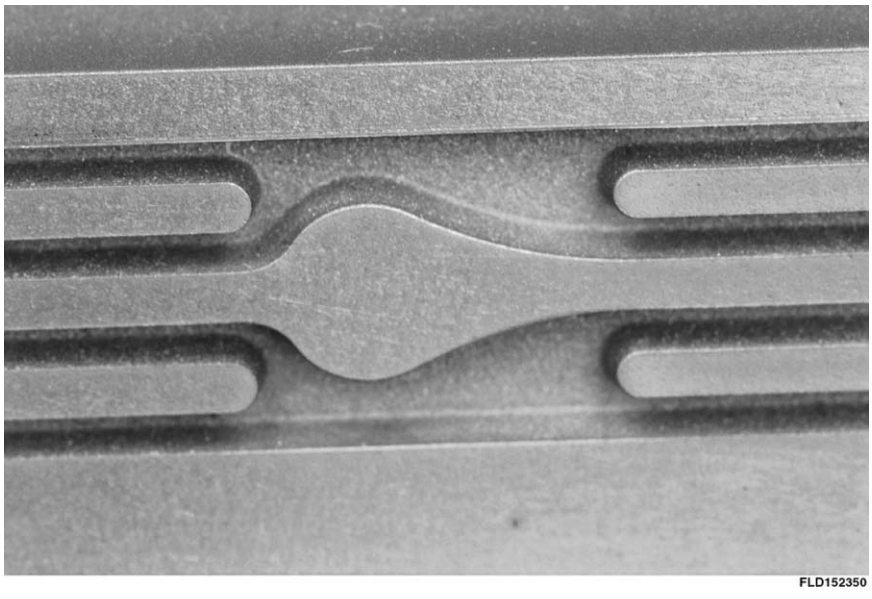

Figure 8 Fuel cooled structure—inconel plate with water-jet machined flow passages.

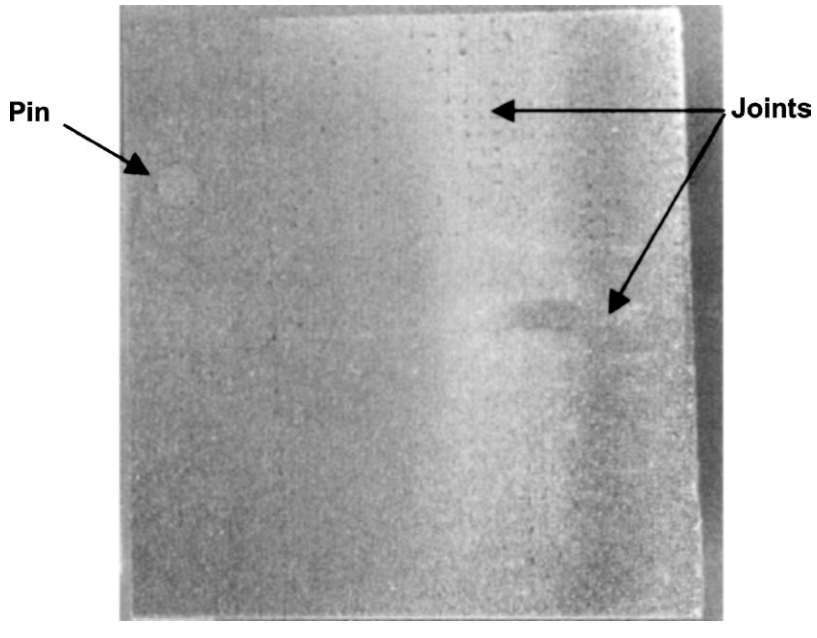

Figure 9 Scramjet leading edge test sample. Pinned, three-piece, C/SiC structure. Post Mach 4.8 test.

material and process solutions would enhance scramjet performance and durability.

3.1. Heat flux amplification

The heat flux to the engine structure is estimated by the local flow conditions. The initial design of the heat exchanger (fuel-cooled structure), the required local fuel flow rates, and the flight conditions associated with the balance point between structural cooling and engine fuel flow requirements is determined by these conditions. Local heating is, however, amplified by the presence of a shock in the flow field and by localized flame holding.

Shocks of various strengths are pervasive in the scramjet flow path. Fig. 10 contains two Schlieren images of shocks in an engine isolator. At the Mach 4 flight condition the throat Mach number is approximately 1.94. With the high back pressure induced by combustion the isolator flow slows to subsonic speeds through a series of normal shocks. At flight Mach number near 6, the throat is at Mach 2.86. Combustor flow remains supersonic, but is slowed through a series of oblique shocks. In either case the wall flow is dramatically affected by the presence of the shock and its interaction with the local wall boundary. The local heat flux can be amplified by several times over that obtained by using the one dimensional flow values.

Similarly, combustion in a scramjet can be very localized with flameholding occurring behind a fuel injection site or downstream of a shock impinging on a wall. Locally the heat flux to the combustor wall can exceed substantially that predicted by integral analysis.

The shocks' position and strength (see Fig. 10), and the location and intensity of discrete flame zones change with flight conditions. Inconel's thermal

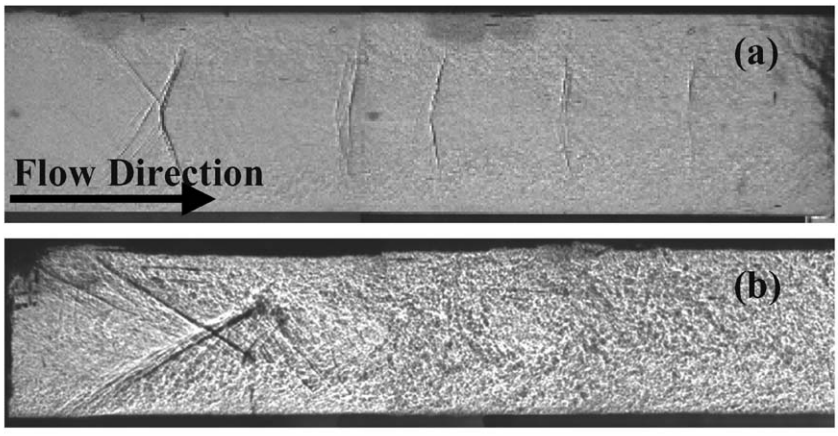

Figure 10 Shadowgraph of simulated pre-combustion shock train contained within scramjet isolator. (a) Flight Mach number 4, throat Mach number 1.94; (b) Flight Mach number 6, throat Mach number 2.86.

conductivity is low. Severe local heating forces the back-side cooling fuel flows to be high-significantly higher than the average heat flux requirements dictate. A material or structural system that had high conductivity along the gas-side surface, but low conductivity normal to the surface would mitigate the thermal problem due to shock amplification.

3.2. Maintaining tight tolerances in critical areas

Scramjet engine flow lines are relatively simple in design. However, engine performance is sensitive to the flow lines. Deviations from the nominal flow lines due to thermal stresses during engine operation and cycling or due to machining tolerance can impact performance. To illustrate the performance sensitivity to material deformations, a series of calculations was performed for a two-dimensional model of an engine isolator. The isolator is a near-constant area duct separating the scramjet inlet and combustor; its purpose is to contain the shock train generated by the pressure rise within the combustor, thus preventing inlet unstart.

The length and height of the computational domain was 1.016 and 0.0508 m, respectively. The inflow conditions were: $M = 2$; $P = 100$ kPa; $T = 800$ K. All calculations were performed with the VULCAN Navier-Stokes Solver [8]. In this study the low diffusion flux vector split scheme of Edwards [9] was employed with the Van Leer flux limiter and MUSCL parameter set equal to 1/3 to minimize truncation error. The solutions were advanced in time with a diagonalized approximate factorization scheme [10]. Turbulence was modeled with the Menter BSL two-equation turbulence model [11]. At solid surfaces, the wall matching procedure of Wilcox [12] was employed. A solution for supersonic flow through the domain was first obtained using the Parabolized Navier-Stokes (PNS) solver. Secondly, a back pressure of 400 kPa was then applied. The calculation was advanced with the CFL (Courant, Friedrichs and Lewy) number of 3.0 and continued until the residual dropped six orders of magnitude, which typically required 25000 iterations.

The dimensions of the grid were 201 $\times$ 41 in the streamwise and normal directions, respectively. The distance from the wall to the first grid point equaled 0.0127 cm and approximately yielded a turbulent inner law variable, $y^+ = 15.0$. This value was chosen to minimize the error associated with the use of wall functions. Solutions were also obtained with a grid containing 31, 81 and 101 points in the normal direction. The shock train location was nearly identical for solutions on all four grids. The grid has a deformation on the top wall extending from $x/H = 10.8$ to $x/H = 11.8$, Fig. 11. The effect of both the location and size of the deformation was investigated.

The solution for the case without a deformation was first obtained. Shown in Fig. 12 are the velocity vectors in the vicinity of the shock train shaded by the static pressure. The series of shock wave, expansion wave, and shock wave corresponding to the flow turning into itself at the beginning of the recirculation zone, away from itself near the back of the recirculation zone and then into itself to become parallel to the wall is observed. The peak pressure ratio (maximum pressure divided by the average pressure at the inflow plane) along the centerline of the duct is equal to 3.69 (438.0 kPa/118.7 kPa) or 92% of the normal

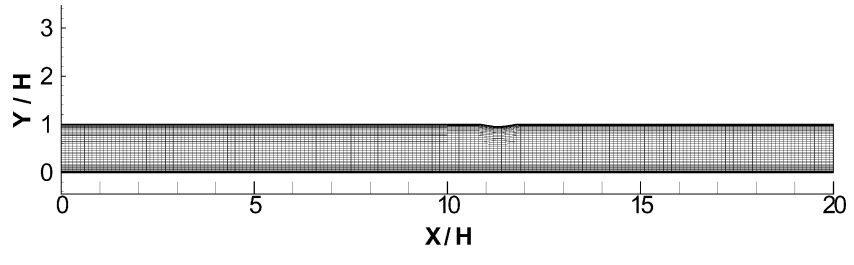

Figure 11 Computational grid with flow surface defect at $x/H = 10.8$.

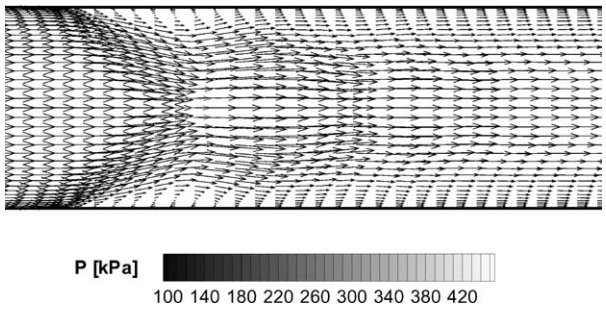

Figure 12 Isolator pressure field with no wall defect.

shock pressure rise for the local approach Mach number of 1.89.

Deformations with a maximum displacement of 0.254 cm or 0.050 H were considered at eight axial locations with the beginning of the deformation at $x/H = 2.95$, 4.92, 6.89, 8.86, 10.83, 12.80, 14.76 and 16.73. The shock train for the geometry without a deformation begins at $x/H = 12.7$. The inflow is uniform and the boundary layer grows nearly linearly with x. At $x/H = 12.7$ the boundary layer thickness, displacement thickness and momentum thickness are 1.06 cm, 0.21 cm and 0.075 cm, respectively. The deformation located downstream of the nominal shock train location had minimal impact on the flow field. However, the deformation located upstream of the nominal shock train location significantly modifies the shock location. The deformation beginning at $x/H = 10.83$ anchors the shock position in the latter extent of the deformation. When the deformation is located well upstream of the nominal shock position, a series of shock and expansion waves emanates from the forward and backward facing surfaces of the deformation, which may influence the position of the shock train. The position of the shock train for the deformations between $x/H = 2.95$ and $x/H = 8.86$ varied between 10 and 11 duct heights from the inflow plane. Overall, a deformation with a maximum deflection of 0.254 cm caused the shock position to move between 1.5 and 2.5 duct heights if located upstream of the nominal shock position.

The impact of the size of the disturbance was investigated by reducing the maximum deflection from 0.254 to 0.127 cm and 0.0635 cm. Shown in Fig. 13 are the static pressures along the top wall, non-dimensionalized by the inflow pressure, for the case without a deformation and for the three deformations each located at $x/H = 10.8$. The gradual pressure rise upstream of $x/H = 10$ is due to the growth of the boundary layer, while the waviness is due to weak waves generated at the inflow corners from the initiation of the boundary layer. Also, the pressure rise due to the shock train is observed to be monotonic. The smallest deflection, $\Delta y = 0.0635$ cm, which is approximately the same size as the momentum thickness does not change the shock position. However, deflections of 0.127 and 0.254 cm both cause the shock train to attach to the deformations moving the shock train approximately 1.5 duct heights upstream. Proper sizing of the engine isolator is essential as this component contributes to engine operability, not thrust, and represents weight and area to be cooled.

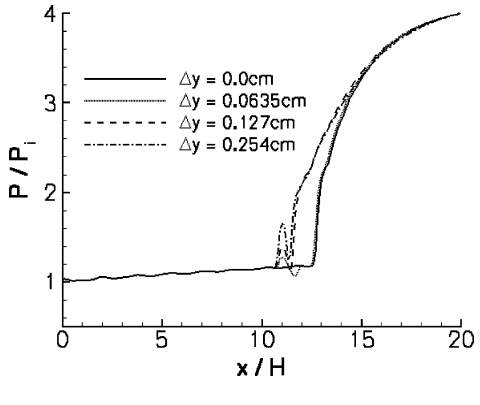

Figure 13 Non-dimensional wall pressure distributions for different sized wall defects.

3.3. Extending the flight mach number limit of hydrocarbon fuels

For many applications of hypersonic propulsion systems hydrocarbon fuels are attractive. They are easy to handle, are easily stored as liquid, and package well in a flight vehicle due to their high volumetric energy content.

The current flight Mach number limit for hydrocarbon fuels is governed by the thermal balance, i.e., matching the cooling load to the thermal capacity of the fuel. Extending the flight Mach number beyond 8 will depend on reducing the surface area, increasing the fuel thermal capacity, reducing the heat transfer rate to the wall (e.g., transpiration cooling), and developing higher temperature materials.

3.4. Light weight/high temperature structures

Ceramic Matrix Composite Structures (CMCS) have potential as fuel-cooled structural material. Carbon/silicon carbide (C/SiC) is an example. The benefits resulting from successfully utilizing CMCS for the combustor structure are two-fold. They have a lower thermal conductivity and lighter weight when compared to similar metallic concepts. The lower thermal conductivity could extend the operational Mach number, while staying within the thermal margin of the endothermic fuel. A combustor wall of this material could be manufactured in the same way that the metallic walls are made, Fig. 14. The only difference is that a backside panel is

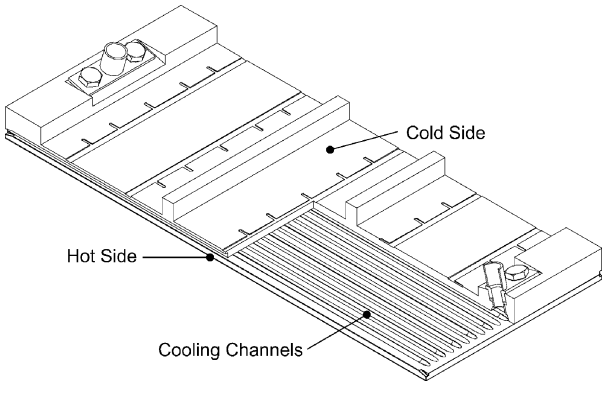

Figure 14 Fuel cooled C/SiC structure.

brazed to the panel with the cooling channels instead of welded, as in the case of the inconel structure. The limiting conditions of a C/SiC structure in this configuration is the hot face temperature and the braze temperature.

While the benefits of using such a material are attractive, there are certain challenges that must be overcome. The most notable problem with this material is its porosity. Adequate sealing techniques must be employed to satisfy operational, safety and storage requirements of the vehicle in order to make fuel-cooled ceramics a viable alternative to metallic structures.

4. Summary/conclusions

Scramjet engine technology has matured over more than 4 decades, yet no scramjet engines have been put into service nor significantly demonstrated in flight. Progress has been substantial in demonstrating critical features of the engine in ground testing. This includes ignition and sustained operation over a wide range of Mach numbers. Sustaining an acceptable thermal balance within the structure has also been demonstrated for limited life propulsion systems. Enabling technologies for maintaining this balance in a hydrocarbon fueled scramjet include endothermic fuels, water-jet machining and laser welding of inconel structures, and certain high temperature materials that can operate uncooled without deformation. These technologies have made the scramjet viable for expendable applications and ready for flight demonstration. More aggressive material advances to raise operating temperatures and maintain critical dimensions; progress in advanced endothermic fuels to raise their heat sink capacity; and more progress in high speed aerodynamics to minimize cooled surfaces are required for developing reusable, longer-use hypersonic propulsion systems.

Acknowledgements

The coauthors wish to thank Dr. Mark Gruber, senior researcher in the experimental group within the Aerospace Propulsion Division for analysis of the scramjet flight corridor and the station-by-station analysis of the Air Force research flow path.

References

1. R. MERCIER and C. McCLINTON, "Hypersonic Propulsion—transforming the Future of Flight," AIAA 2003-2732 (2003).
2. I. M. BLANKSON, Presentation to the U.S.A.F. Scientific Advisory Board (1991).
3. A. C. NIXON, G. H. ACKERMAN, R. D. HAWTHORNE, A. W. RICHIE, H. T. HENDERSON and I. S. BJORKLND, "Vaporization and Endothermic Fuels for Advanced Engine Applications," AFAPL TDR 64-100 (1964) Parts I, II, and III.
4. A. C. NIXON, G. H. ACKERMAN, L. E. FAITH, R. D. HAWTHORNE, H. T. HENDERSON, A. W. RICHIE, L. B. RYLAND and T. M. SHRYNE, "Vaporization and Endothermic Fuels for Advanced Engine Applications," AFAPL TDR 67-114 (1967) Parts I, II, and III.
5. H. HUANG, D. R. SOBEL and L. J. SPADACINNI, "Endothermic Heat-Sink of Hydrocarbon Fuels for Scramjet Cooling," 38th AIAA/ASME/SAE/ASEE Joint Propulsion Conference, AIAA 2002-3871 (2002).
6. K.-C. LIN, P. J. KENNEDY and T. A. JACKSON, "Structures of Internal Flow and the Corresponding Spray for Aerated-Liquid Injectors," AIAA 2001-3569 (2001).
7. K.-C. LIN, S. COX-STOUFFER, P. J. KENNEDY and T. A. JACKSON, "Expansion of Supercritical Methane/Ethylene Jets in a Quiescent Subcritical Environment," AIAA 2003-0483 (2003).
8. J. A. WHITE and J. H. MORISSON, "Pseudo-Temporal Multi-Grid Relaxation Scheme for Solving the Parabolized Navier-Stokes Equations," AIAA Paper 99-3360 (1999).
9. J. R. EDWARDS, *Comp. and Fluids* **26**(6) (1997) 635.
10. T. H. PULLIAM and D. S. CHAUSSEE, *J. Comp. Phys.* **39** (1981) 347.
11. F. R. MENTER, "Zonal Two Equation k-ω Models for Aerodynamic Flows," AIAA Paper 93-2906 (1993).
12. D. C. WILCOX, "Wall Matching, a Rational Alternative to Wall Functions," AIAA Paper 89-0611 (1989) .

Received 10 October 2003
and accepted 8 March 2004